SPECTRUM OF ENGINEERING SCIENCES
ISSN (E) 3007-3138 (P) 3007-312X VOLUME 4, ISSUE 6, 2026

SYNTHESIS AND STRUCTURAL CHARACTERIZATION OF AL-$TI_3C_2T_x$ MXENE DERIVED FROM TI_3ALC_2 MAX PHASE AS A PLATFORM FOR REGENERATIVE LACTATE BIOSENSING

Zain-ul-Abideen[1], Dr. Wasif Mehmood Ahmed Malik[*2], Muhammad Mohsin[3], Dr. Adeel Hussain Chughtai[4], Wamiq Rao[5]

[1,4,5]*Institute of Chemical Sciences, Bahauddin Zakariya University, Multan-60800, Pakistan.*
[*2]*Lecturer Emerson University Multan, Pakistan.*
[3]*HOD of chemistry Aspire college Adda Zakhera Tehsil Dunyapur district Lodhran, Pakistan.*

[1]zk6442278@gmail.com, [*2]wasif.mehmood@eum.edu.pk, [3]emersonlord143@gmail.com, [4]adeelhussain@bzu.edu.pk, [5]rwamiq42@gmail.com

DOI: https://doi.org/10.5281/zenodo.21099676

Keywords
$Ti_3C_2T_x$ MXene; Ti_3AlC_2 MAX Phase; Lactate Biosensor; Regenerative Biosensing; Electrochemical Sensing; Lactate Oxidase; Cyclic Voltammetry; Structural Characterization; Two-Dimensional Nanomaterials; Biomedical Diagnostics.

Article History
Received: 25 April 2026
Accepted: 04 June 2026
Published: 21 June 2026

Corresponding Author: *
Dr. Wasif Mehmood Ahmed Malik

Abstract

In the present study, Al–$Ti_3C_2T_x$ MXene was synthesized from Ti_3AlC_2 MAX phase, and its structure was characterized before electrochemical characterization was performed to assess its potential application in regenerative lactate biosensing. Al–$Ti_3C_2T_x$ MXene was prepared by selectively etching Ti_3AlC_2 with hydrofluoric acid, washing, exfoliation and purification. The transformation of the structure from the parent MAX phase to MXene phase was systematically studied with the aid of X-ray diffraction (XRD), scanning electron microscopy (SEM) and energy-dispersive X-ray spectroscopy (EDS).

The XRD spectrum showed the shift of characteristic diffraction peak (002) to lower diffraction angle and the decrease in the intensity of the higher order reflections, which indicated a successful exfoliation of aluminum layers and expansion of interlayer spacing. SEM images revealed a typical multi-layered structure with expanded galleries between the layers, and elemental mapping and EDS analysis confirmed the presence of only Ti and C with O- and F-containing terminations on the surface and a negligible amount of residual aluminum. Lactate oxidase (LOx) was immobilized onto the surface of the synthesized MXene, after which an electrochemical characterization of the immobilized enzyme was performed using cyclic voltammetry.

The current response to lactate was found to be concentration dependent, the Al–$Ti_3C_2T_x$–LOx bioelectrode has better electron-transfer activity, a high selectivity to common interfering species, and excellent operational stability. The biosensor showed maximum response at physiological pH (7.0) and it also showed efficient charge transfer and surface-controlled electrochemical process. The linear range for detection was 10 – 90 μM, the sensitivity was 0.017 μA μM^{-1}, the limit of detection (LOD) was 2.5 μM and the limit of quantification (LOQ) was 8.3 μM, as found from quantitative analysis. The advanced material platform of Al–$Ti_3C_2T_x$ MXene is suggested by its high conductivities, enlarged interlayer spacing, abundant functional groups, and favorable electrochemical properties for

its potential use in lactate biosensing in a regenerative manner and in future biomedical monitoring applications.

1 Introduction

In view of the rapidly growing demand for fast, sensitive and reliable biosensing technology, there are growing efforts to develop advanced functional nanomaterials in the healthcare and biomedical fields [1]. Lactate has attracted a great deal of interest as a biomarker because of its crucial involvement in cell processes, tissue regeneration, wound healing, monitoring of physical performance and diagnosis of disease [2]. Lactate is a key parameter to assess physiological or pathological situations such as hypoxia, sepsis, cancer progression, cardiovascular diseases or metabolic dysfunction [3, 4]. In addition, lactate monitoring has been found to be useful in regenerative medicine, where the real-time measurement of cellular metabolic functions can help understand tissue repair, stem cell function and therapeutic responses [5, 6]. Thus, the design and construction of highly efficient lactate biosensors with rapid and precise detection are still a research topic of interest in the biomedical field [7, 8].

Although the conventional lactate biosensors have been used in clinical diagnosis with great success, they still suffer from a number of limitations, such as insufficient sensing sensitivity, poor electron-transfer kinetics, narrow detection range, and decreased operating stability [9, 10]. These restrictions have spurred the development of nanostructured materials for improvement of the electrochemical response and sensing performance [6, 11]. Nanomaterials like graphene, carbon nanotubes, metal nanoparticles, conducting polymers and transition metal oxides have been extensively studied in the field of biosensing in recent years [12]. However, some issues such as conductivity, biocompatibility, surface functionalization and stability persist and limit their use in next generation regenerative biosensing systems [8].

MXenes have been the subject of remarkable research interest as emerging 2D nanomaterials, due to their peculiar physicochemical features [13]. MXenes are a class of transition metal carbides, nitrides and carbonitrides, in general, can be represented as $M_{n+1}X_nT_x$, where M stands for an early transition metal, X can be carbon and/or nitrogen and T_x represents surface termination groups like –OH, –O and –F [14, 15]. Ever since their discovery, MXenes have shown to possess high hydrophilicity, tunable surface chemistry, excellent mechanical flexibility, large specific surface area, and an outstanding electrical conductivity [16]. These properties have led to their use in many applications such as energy storage, catalysis, environmental remediation, electromagnetic shielding, wearable electronics and biosensing technologies [17].

$Ti_3C_2T_x$ is the most widely studied MXene composition so far reported because it is easy to synthesize, possesses excellent electrical conductivity, and has good electrochemical properties . The $Ti_3C_2T_x$ is generally formed by selective etching of aluminum layers from the Ti_3AlC_2 MAX phase, which yields a two-dimensional structure composed of layers with numerous functional groups on the surface [18]. Removal of the aluminum provides increased interlayer spacing, and it creates active sites that can provide for efficient charge transfer and biomolecule immobilization. Such features make $Ti_3C_2T_x$ MXene an attractive electrochemical biosensor material because electron transport is fast and there are good interactions at the interface between the material and the bio-electrolyte, which are important for high analytical performance [19].

The outstanding electrical conductivity and rich surface chemistry of MXenes, $Ti_3C_2T_x$, has great potential for lactate biosensing applications [20]. The large surface area provides high enzyme loading capability and biomolecular interactions, and the conductive layered structure allows for fast electron transport between the biomolecular recognition elements and the surface of the electrode. Furthermore, the functional groups, including oxygen, hydroxyl and fluorine, enhance the hydrophilicity and offer good functional groups for biochemical functionalization [20]. The

properties are especially useful for regenerative biosensing platforms where continuous and sensitive monitoring of metabolic biomarkers is required in complex biological conditions [21].

Although many significant developments have been achieved in the field of MXenes-based biosensors, the correlation between the synthesis conditions, MXene structure, and sensing performance is still under investigation [16]. Full characterization of MXene materials is necessary to account for structural changes which take place during the conversion of Ti3AlC2 MAX phase to MXene Ti3C2Tx and to assess the potentials for biosensing applications [22]. The electrochemical behavior and the sensing efficiency is strongly influenced by structural parameters like crystallinity, morphology, elemental composition, interlayer spacing and surface functionalization [23, 24].

For this reason, in the present study, Al-$Ti_3C_2T_x$ obtained by a selective etching strategy of the Ti_3AlC_2 MAX phase is synthesized and characterized in detail by the X-ray diffraction (XRD), scanning electron microscopy (SEM), and energy-dispersive X-ray spectroscopy (EDS) techniques. Parent MAX phase to exfoliated MXene phase structural evolution is systematically investigated to assess formation of functionalized $Ti_3C_2T_x$ layers [25]. Second, the physicochemical properties obtained are discussed with respect to their potential use as a promising biosensor platform for the regenerative lactate sensing. The results offer crucial information that will be used to develop the next generation of advanced MXene-based materials for future biomedical sensing technologies and regenerative healthcare systems [26].

2 Materials and Methods

2.1 Materials

The Ti_3AlC_2 MAX phase was used as the precursor material to synthesize $Ti_3C_2T_x$ MXene. The selective etching agent was hydrofluoric acid (HF) to remove the aluminium layers from the MAX phase. Throughout washing and purification processes, deionized water was used. All of the chemicals used in this study were analytical grade and used without any further purification.

2.2 Synthesis of Al-$Ti_3C_2T_x$ MXene

Al-$Ti_3C_2T_x$ MXene was prepared by selective chemical etching of Ti_3AlC_2 MAX phase and exfoliation/purification. The synthesis process was designed so as to eliminate the aluminum atomic layers from the parent MAX structure while keeping the titanium carbide framework that forms two-dimensional MXene sheets intact [27].

1.0 g of Ti_3AlC_2 MAX phase powder was gradually added to 20 mL of hydrofluoric acid (HF, 40 wt%) while stirring it constantly with magnetic stir. The addition was carried out slowly to prevent too much heat being generated, and to facilitate the even interaction of the precursor particles with the etching medium. The obtained suspension was stirred for a period of 24 h at room temperature to selectively dissolved the aluminum layers of the Ti_3AlC_2 structure. During the etching process, the Al atomic layers were removed and the resulting multilayered $Ti_3C_2T_x$ MXene consisted of functional groups of –O, –OH, –F groups on the surface [28].

After etching the reaction was washed with deionized water several times and centrifuged at 3500 rpm for 5 minutes each time with deionized water. The washing process was repeated until the pH of the supernatant was about 6–7, which was considered to be a sign of the successful removal of the remaining acid and reaction products. The purification process is vital in order to enhance the stability and electrochemical characteristics of the synthesized MXene.

Then the purified sediment was spread in deionized water and treated under ultrasonic conditions for 60 minutes to delaminate the multi-layers of MXene stacks into thinner nanosheets. The penetration of water molecules between adjacent layers, which was assisted by ultrasonication, led to an increase in the interlayer spacing and better exfoliation of the $Ti_3C_2T_x$ structure.

The suspension was then centrifuged at 3500 rpm for 30 min after the exfoliation to remove unetched particles and thicker multilayer

aggregates from the exfoliated MXene nanosheets. The supernatant was retained and dried in a vacuum oven at 60 °C for 12 h, to collect the delaminated Al-$Ti_3C_2T_x$ MXene. The product obtained was in the form of dark gray powder and was kept in covered containers until characterization.

The selective removal of aluminium from the Ti_3AlC_2 MAX phase led to the formation of a layered structure of $Ti_3C_2T_x$, with enlarged interlayer spacing, numerous surface functional groups and a high specific surface area. The electron transfer and biomolecule immobilization properties of the synthesized Al-$Ti_3C_2T_x$ MXene are very attractive, which renders it as a potential material in the field of regenerative lactate biosensor applications [29].

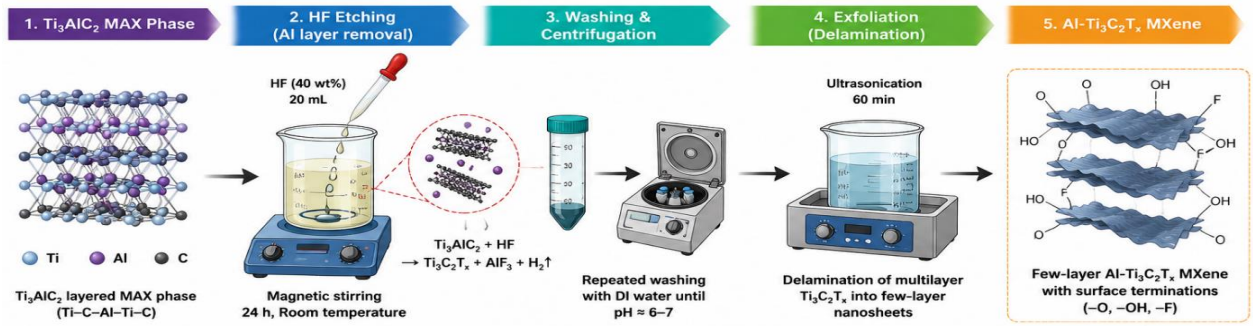

Figure 1: Schematic illustration of synthesis process

2.3 Structural Characterization

The crystallographic structures of the precursor Ti_3AlC_2 MAX phase and the synthesized Al-$Ti_3C_2T_x$ MXene was investigated by X-ray diffraction (XRD). The diffraction patterns were collected on a suitable 2θ range for assessing the phase composition, crystallinity, and structural changes during the etching process. Changes of diffracted peak positions and intensities were examined to ensure that the transformation of the MAX phase to MXene was successful.

The surface morphology and microstructural features of the synthesized materials were studied by the aid of scanning electron microscopy (SEM). The SEM analysis gave information on the exfoliation of layers, the texture of the surface and the morphological changes caused by the removal of the aluminum layers. Images were obtained at different magnifications to evaluate the formation of characteristic layered MXene structures.

Elemental composition and elemental distribution were studied with the help of energy-dispersive X-ray spectroscopy (EDS) coupled with SEM. The elemental analysis was done to confirm the presence of Ti, C, O and F, and to assess the degree of Al removal following etching. Elemental mapping was also performed to locate the spatial distribution of constituent elements in the synthesized MXene structure [30].

2.4 Potential Application in Regenerative Lactate Biosensing

Physicochemical properties of the synthesized Al-$Ti_3C_2T_x$ MXene were found to be an excellent material platform for the regenerative lactate sensing application. The unique structure of MXenes offers many surfaces functional groups, a large active surface area, and high electrical conductivity, making it an ideal structure for biomolecule immobilization and efficient electron transfer. It is hoped that these properties will increase the sensitivity, response speed and stability of lactate sensing systems. The structural properties derived from the XRD, SEM and EDS analysis were thus evaluated in terms of potential application as a regenerative biosensor.

3 Results and Discussion

3.1 XRD Analysis of Ti_3AlC_2 MAX Phase and Al-$Ti_3C_2T_x$ MXene

The X-ray diffraction (XRD) patterns of the pristine Ti_3AlC_2 MAX phase and synthesized Al-$Ti_3C_2T_x$ MXene are shown in Figure 2. The diffraction pattern of Ti_3AlC_2 shows a set of well-defined and sharp peaks, which suggests its highly crystalline nature. The characteristic reflections observed at approximately 2θ = 9.5°, 19°, 30°, 36°, 39°, 42°, 48°, 57°, and 61° can be indexed to the (002), (004), (101), (103), (104), (105), (107), (108), and (110) crystallographic planes, respectively. These peaks are very strong diffraction peaks that confirm the formation of the layered hexagonal structure of Ti_3AlC_2, and are in good agreement with the diffraction patterns reported for MAX phases.

It is found that the XRD pattern of the etched Al-$Ti_3C_2T_x$ MXene changes significantly after the selective etching of the Al layer. The most noticeable is the strong diffraction peak at a lower diffraction angle with a much higher intensity than the parent MAX phase, corresponding to the (002) reflection. The change of the (002) reflection towards the lower 2θs values is related to the increase of the interlayer spacing (d-spacing), which has been attributed to the removal of Al atomic layers, and to the subsequent insertion, of surface termination groups like –OH, –O, and –F. The widening interlayer spacing is regarded as a structural signature of the formation of $Ti_3C_2T_x$ MXenes. In addition, the diffraction peaks of the higher-order planes of the MAX phase show a significant decrease in intensity or are considerably broadened following etching. These reflections are attenuated, suggesting a loss of long-range crystallographic order in the sample caused by the exfoliation process and the surface functional groups formed [31].

Peak broadening is also linked to reduced crystallite size and increased structural disorder which are typical features of MXene materials prepared by chemical etching. The disappearance of several characteristic peaks of the MAX phase further proves the efficient extraction of aluminum from the Ti_3AlC_2 lattice. At the same time, the preservation of the strong (002) reflection proves that the titanium carbide layers are not affected by etching, ensuring the successful formation of a 2D $Ti_3C_2T_x$ structure [32].

There have been numerous reports of similar structural changes occurring in $Ti_3C_2T_x$ MXenes prepared by etching in HF, and the appearance of the (002) peak accompanied by a decrease of higher angle reflections is regarded as clear proof of MXene formation. An enlarged interlayer distance and functionalization of the surface of the Al-Ti3C2Tx MXene is of particular benefit for electrochemical and biosensing applications. The increased layered structure enables fast transport of ions and electrons and the numerous surface terminations offer binding sites for biomolecule immobilization for a platform for regenerative lactate biosensing.

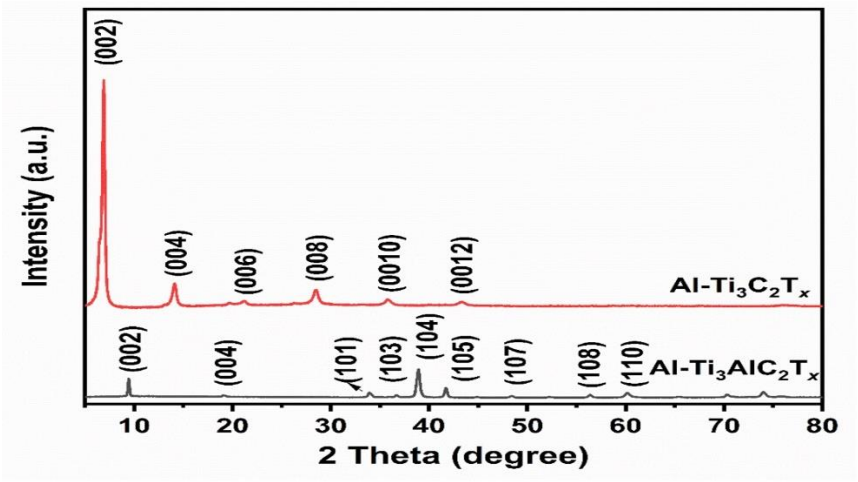

Figure 2 :X-ray diffraction patterns of pristine Ti_3AlC_2 MAX phase and synthesized Al-$Ti_3C_2T_x$ MXene showing the shift of the (002) peak, reduction of higher-order reflections, and structural transformation after selective etching of aluminum layers.

3.2 SEM Analysis of Ti_3AlC_2 MAX Phase and Al-$Ti_3C_2T_x$ MXene

The surface morphology of the pristine Ti_3AlC_2 MAX phase and the synthesized Al-$Ti_3C_2T_x$ MXene were studied using scanning electron microscopy (SEM) and the corresponding electron micrographs are presented in Figure 3. The SEM images show the highly significant morphological changes upon selective removal of the aluminum layers from the parent MAX phase, demonstrating the success of transformation to a layered MXene structure. Figures 3(a) and 3(b) show the surface morphology of the pristine Ti_3AlC_2 MAX phase at magnifications corresponding to scale bars of 10 µm and 1 µm, respectively.

The images display a relatively smooth morphology of the layers, compact layers with dense grains and well-arranged lamellar structures. Surface is continuous and has a low porosity with only minor wrinkles at the margins of the layers. The morphology is representative of the Ti_3AlC_2 MAX phase in which the aluminium layers are tightly connected between the titanium carbide sheets, creating a very rigid and ordered structure. There is no apparent exfoliation, and the layers are compactly packed together, suggesting high crystallinity and structural integrity to the parent material. Substantial changes in morphology of synthesized Al-$Ti_3C_2T_x$ are noticed after chemical etching using hydrofluoric acid, as evidenced in Figure 3(c) and (d) [33].

The SEM images show a distinct and clear structure of a multilayered accordion-like arrangement composed of many stacked and partly delaminated nanosheets. The layers are loosely packed and have larger interlayer spacing than that of the parent MAX phase. This characteristic morphology is due to the selective removal of aluminium atoms from Ti_3AlC_2, which reduces the inter-layer interactions and makes it easier to separate adjacent layers of titanium carbide. When viewed at lower magnifications (Figure 3c), the MXene has a more expanded layered structure, featuring open channels and randomly distributed irregular voids. Such features have been linked to the successful etching and exfoliation of the MAX phase, which results in a remarkable increase of the surface area [32].

A characteristic feature of the open galleries between the adjacent sheets is the high rate of ion diffusion and the large number of available surface reaction sites, which are important for electrochemical applications. The SEM image at high magnification (Figure 3d) also clearly shows the lamellar structure of Al-$Ti_3C_2T_x$ MXene. Each nanosheet can be clearly identified and is stacked in layers, with gaps between them. The layers are

thin and flexible in the shape of a sheet, and have smooth surfaces with little structural collapse, suggesting that the titanium carbide framework is not destroyed by etching. The increase in interlayer spacing noted in the image is in good agreement with the XRD data, which revealed a decrease in the 2θ value of the (002) diffraction peak with the removal of the aluminum layers and the addition of surface termination groups.

The accordion-like morphology and interlayer spacing expansion are some of the key structural features of $Ti_3C_2T_x$ MXenes. These features not only expand the surface area that is available for electrochemical reactions but they also help to transfer charges and masses during electrochemical processes. Furthermore, abundance of edge sites and large exposed surface offer a promising platform for the immobilization of biomolecules/enzymes for biosensing applications. It is confirmed that the aluminum layers are efficiently removed and a two-dimensional MXene architecture with improved surface characteristics is formed, with the transformation from a compact layered structure to an exfoliated accordion-like morphology. The presence of these structural features is anticipated to greatly influence the electrochemical properties and regenerative lactate biosensing capability of the synthesized material .

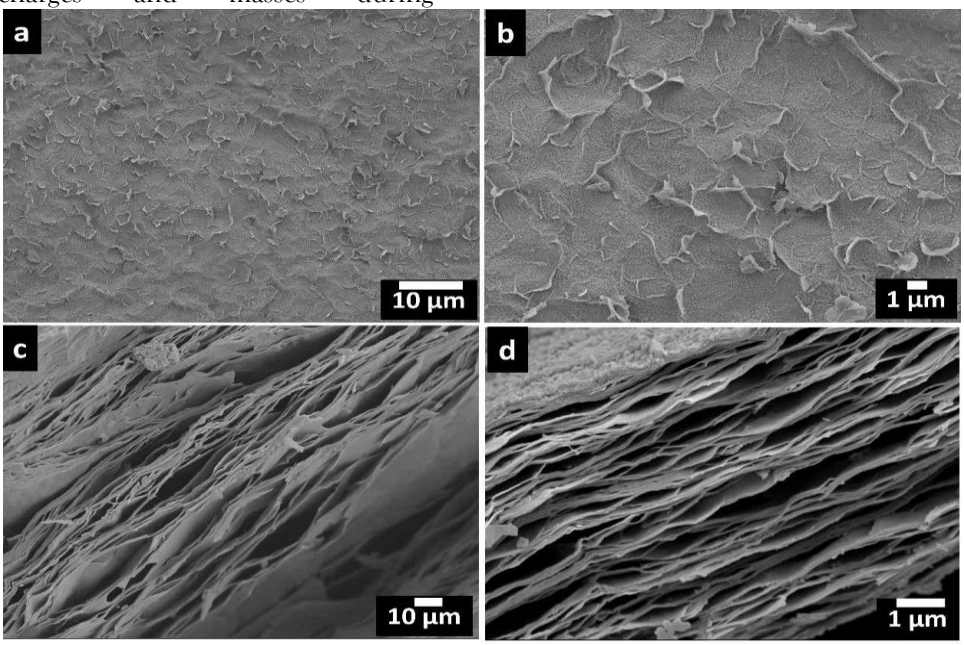

Figure 3: SEM images of Ti_3AlC_2 MAX phase and Al-$Ti_3C_2T_x$ MXene: (a) Ti_3AlC_2 at 10 µm scale, showing compact layered morphology; (b) Ti_3AlC_2 at 1 µm scale, exhibiting a smooth and dense surface; (c) Al-$Ti_3C_2T_x$ MXene at 10 µm scale, revealing an accordion-like expanded structure; and (d) Al-$Ti_3C_2T_x$ MXene at 1 µm scale, showing stacked multilayer nanosheets with enlarged interlayer spacing.

3.2 EDS Analysis of Al-$Ti_3C_2T_x$ MXene

The element composition of the synthesized Al-$Ti_3C_2T_x$ MXene was analyzed by energy-dispersive X-ray spectroscopy (EDS) and the result is shown in Figure 4. The EDS results give useful information about the elemental composition of the synthesized material, and demonstrate the transformation of Ti_3AlC_2 MAX phase into $Ti_3C_2T_x$ MXene during selective chemical etching. The EDS spectrum as presented in Figure 4, shows that the synthesized material is mainly composed of the element titanium (Ti) with an intense peak at around 4.5 keV.

The quantitative analysis shows that Ti has the most concentration which is 67.43% by weight and 46.69% by atom. The abundance of titanium is in good agreement with the chemical composition of $Ti_3C_2T_x$ MXene in which the

basic structure is based on the layers of titanium carbide. The high Ti signals retained after etching indicate the lattice of the TiC is stable during the synthesis.

Carbon (C) is also very well identified in the EDS spectrum, with a characteristic peak at ~0.28 keV. It was determined that the carbon content was 6.88 wt% and 18.99 at% which is indicative of the presence of carbide layers inside the MXene structure. Due to its low atomic mass and thus weight percentage, the weight percentage of carbon is lower than titanium; however, the relatively high atomic percentage means that the contribution of carbon to the Ti_3C_2 lattice is significant. The presence of both Ti and C elements therefore suggests the successful formation of the nanosheets of TiC. The EDS analysis also confirmed the presence of two elements that are typical surface termination groups of chemically etched MXenes: oxygen (O) and fluorine (F).

The weight percentage of oxygen and fluorine were found to be 9.66% and 5.94%, respectively, and the atomic percentage of oxygen and fluorine were 20.03% and 10.37%, respectively. The oxygen peak observed around 0.52 keV is assigned to oxygen functionalities on the surface like –O and –OH groups, while the fluorine signal is due to –F terminations, which are introduced by HF etching. These surface functional groups are a key feature of $Ti_3C_2T_x$ MXenes, as they make them more hydrophilic, stabilize them in dispersion and serve as active sites for further functionalization and immobilization of biomolecules. One of the interesting things that can be noted from the EDS spectrum is that the Aluminum (Al) content is very low.

Only traces of Aluminium (0.06 wt % and 0.07 at % represented by a very weak peak near 1.5 keV) were detected. The small amount of Al suggests that Al layers are effectively removed from the parent Ti_3AlC_2 MAX phase during the HF etching process. Aluminum reduction is regarded as one of the more significant changes to indicate success in the synthesis of MXenes and is reflective of the conversion of the MAX phase into the two-dimensional $Ti_3C_2T_x$ structure.

In addition to the spectrum of gold (Au), the spectrum of chlorine (Cl) also shows up as minor peaks. The weight and atomic percents of gold equal to 7.23% and 1.22% respectively are due to the fact that the sample was coated with gold before SEM-EDS analysis to enhance the electrical conductivity and the quality of the image. In a similar way, chlorine was identified in traces (2.81 wt % and 2.63 at %), which may be a result of the presence of chemicals as residues or minor impurities from the sample preparation and washing. The presence of these minor elements does not significantly influence the integrity or chemical composition of the synthesized MXene.

As a whole, the EDS results validate the presence of mainly Ti, C, and surface terminations containing O and F with the presence of the Al element being almost absent after chemical etching. The elemental composition is also in good agreement with the proposed $Ti_3C_2T_x$ MXene structure, and is a good indicator of successful synthesis of Al-$Ti_3C_2T_x$. The multiple surface functional groups along with the low residual aluminium content indicate that the material has good physicochemical characteristics for electrochemical and biosensing applications, specifically for regenerative lactate sensing.

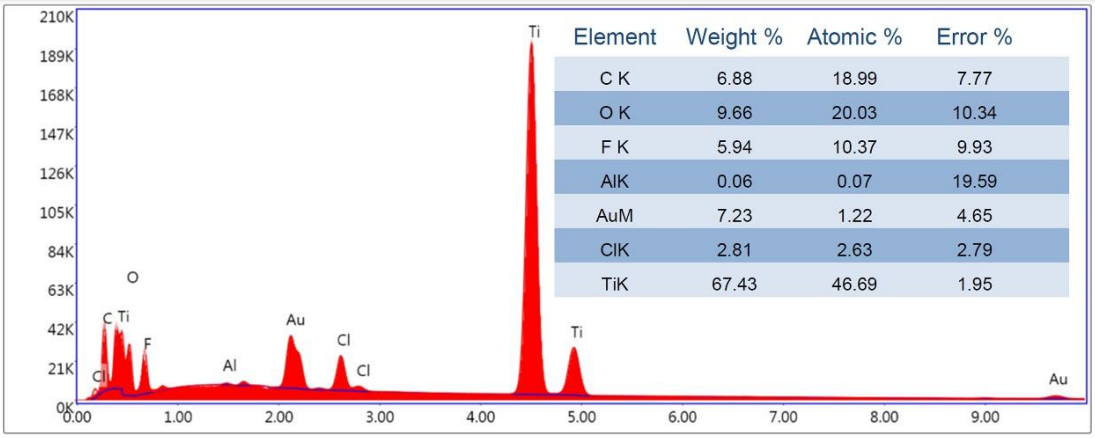

Figure 4: Energy-dispersive X-ray spectroscopy (EDS) spectrum and elemental composition of Al-$Ti_3C_2T_x$ MXene showing the predominant presence of Ti and C along with O- and F-containing surface terminations and negligible residual Al content, confirming the successful conversion of Ti_3AlC_2 MAX phase into $Ti_3C_2T_x$ MXene.

3.3 EDS Elemental Mapping of Al-$Ti_3C_2T_x$ MXene

Energy-dispersive X-ray spectroscopy (EDS) elemental mapping was then used to further investigate the spatial distribution of elements in the synthesized Al-$Ti_3C_2T_x$ MXene. The elemental maps of the carbon (C), oxygen (O), fluorine (F), aluminum (Al), chlorine (Cl), and titanium (Ti) elements are shown in Figure 5. The mapping results not only give important information on the homogeneity of elemental distribution but also further confirm successful synthesis and surface functionalization of $Ti_3C_2T_x$ MXene. The result of chemical etching on the sample is shown in Fig.5, where carbon (C) is distributed uniformly, which means the titanium carbide framework has been preserved after the etching process. The homogeneity of carbon is observed, which ensures the preservation of the carbide layers of the parent Ti_3AlC_2 MAX phase. The lack of carbon-rich/carbon deficient areas also indicates that the etching and exfoliation processes were uniform over the surface of the sample.

The elemental map of oxygen (O) shows that oxygen-containing species are present in all parts of the MXene layers. The oxygen is claimed to be contributed by the oxygen containing surface termination groups like –O, –OH, which are often created by hydrofluoric acid etch and washing. The relatively uniform distribution of oxygen suggests that the surface functionalization was homogeneous, leading to a uniform surface with oxygen-rich active sites throughout the material. The presence of these oxygen containing groups is known to enhance the hydrophilicity and chemical reactivity of MXenes, which is beneficial for biomolecule immobilization in biosensing applications. The elemental map of the same sample for fluorine (F) shows a uniform distribution of the element across the sample surface.

The synthesis of $Ti_3C_2T_x$ MXene in HF results in terminations by fluoride atoms, which become attached to the free titanium surfaces during the etching process. The presence of uniformly distributed fluorine groups validates the successful surface modification of the nanosheets of MXene. These fluorine terminations can give the material increased surface wettability and affect the electrochemical behavior of the material by altering its electronic structure and surface properties.

A small amount of chlorine (Cl) is also detected in the mapping images. The chlorine distribution appears sparse and irregular, suggesting that Cl is present only as a trace impurity or residual species originating from the synthesis or purification processes. The low concentration and non-

uniform distribution of chlorine indicate that it does not constitute an integral part of the MXene structure and is unlikely to affect the overall properties of the synthesized material.

Titanium (Ti), the principal constituent of $Ti_3C_2T_x$ MXene, exhibits a strong and highly uniform distribution across the entire mapped region. The homogeneous dispersion of titanium confirms the preservation of the titanium carbide backbone after selective etching and exfoliation. The absence of Ti-deficient areas indicates the structural stability of the MXene layers and demonstrates that the chemical treatment selectively removed aluminum while maintaining the integrity of the Ti_3C_2 framework.

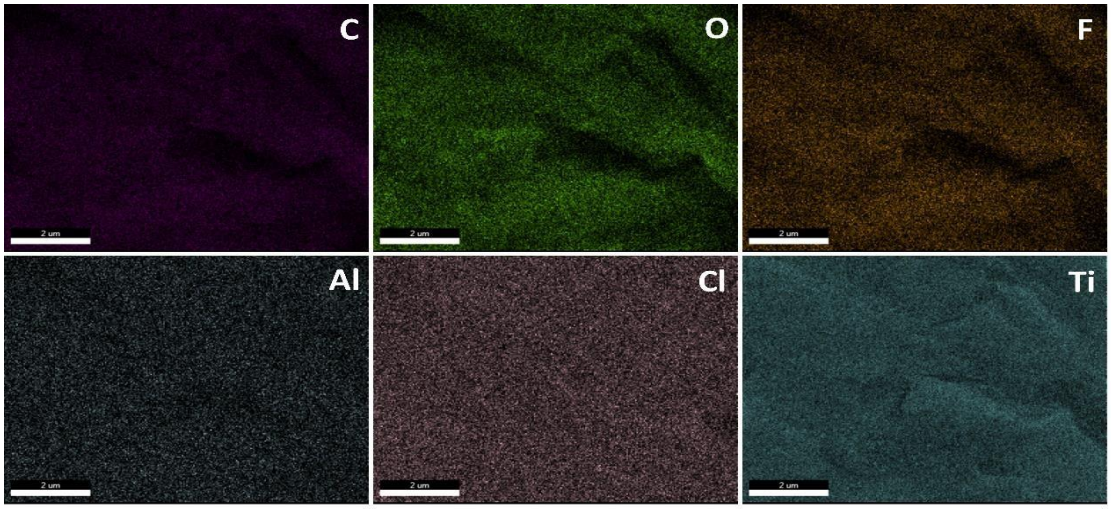

Figure 5 :EDS elemental mapping images of Al-$Ti_3C_2T_x$ MXene showing the spatial distribution of carbon (C), oxygen (O), fluorine (F), aluminum (Al), chlorine (Cl), and titanium (Ti). The homogeneous distribution of Ti, C, O, and F together with the negligible Al signal confirms the successful conversion of Ti_3AlC_2 MAX phase into $Ti_3C_2T_x$ MXene and the formation of surface functional groups.

3.4 Electrochemical Performance of Al–$Ti_3C_2T_x$ MXene-Based Lactate Biosensor

Figure 6 shows the cyclic voltammetric (CV) responses of bare GCE, Al–Ti_3AlC_2 modified GCE and Al–$Ti_3C_2T_x$ modified GCE, as well as the lactate sensing performance, selectivity and operational stability of the Al–$Ti_3C_2T_x$–LOx bioelectrode. The CV curves presented in this figure 6(a) illustrate the effect of the surface modification on the electrochemical behavior of the electrode. Bare glassy carbon electrode (GCE) showed relatively low anodic and cathodic currents, which indicated the low electron transfer ability of the electrode. Modification with the Al-Ti_3AlC_2 MAX phase led to a marked improvement in the current response which indicated better electrical conductivity and better electroactive surface area.

This further and significant rise in the current peak was achieved after the conversion of the MAX phase to Al–$Ti_3C_2T_x$ MXene. The electrode modified by MXenes showed the maximum redox current, which may be explained by the successful removal of Al layer as well as the generation of a two-dimensional layered structure and the presence of a large number of surface terminations (–OH, –O, –F). These structural features enable fast charge transport and offer a high number of active sites for the electrochemical reactions. The synthesized MXene has shown its best electrochemical properties, which is favorable for the application of biosensing on the platform of this material. As shown in Figure 6(b), the CV response of the Al–$Ti_3C_2T_x$–LOx electrode gradually rises with an increasing lactate concentration in the range of 0–10 mM, with both

anodic and cathodic peak currents enhanced as the concentration of lactate rose. This is attributed to the efficient electrocatalytic oxidation of lactate mediated by the immobilized lactate oxidase enzyme.

The progressive rise of the response illustrates progressive bio-recognition and electron transfer process between the reaction products generated by enzymes and the conductive surface of MXene. The increasing of the peak current was well recognized and proportional, indicating a good analytical relationship between the concentration of lactate and the electrochemical signal; this aspect represents a potential application of the developed biosensor for quantitative lactate determination. The maximum current response at 10 mM lactate reveals a wide dynamic sensing range and good catalytic activity of the bioelectrode. The stability and selectivity of the fabricated biosensor are shown in Figure 6(c).

After 50 continuous measurement cycles the CV profile presented a slight reduction in the peak current compared to that obtained in response to initial injection of 10 mM lactate, indicating good electrochemical stability and a good enzyme immobilization on the MXene surface. This behavior suggests that the structure of the electrode does not change and catalytic activity is conserved in repeated use. In addition, the signal of the current response was almost the same in the presence of the common interfering species (uric acid (UA) and ascorbic acid (AA)), as in the presence of lactate itself.

The slight change in peak current indicates the excellent selectivity of the Al–$Ti_3C_2T_x$–LOx biosensor to lactate and the suppression of the interference of electroactive compounds which are often present in biological media. The CV results clearly indicated the excellent conductivity and electrochemically active surface of the Al–$Ti_3C_2T_x$ MXene, which makes it a remarkable platform for immobilization of enzymes to realize sensitive, selective, and stable lactate detection. Overall, the synthesized MXene-based bioelectrode shows great promise for use in lactate biosensing applications, particularly those involving regeneration.

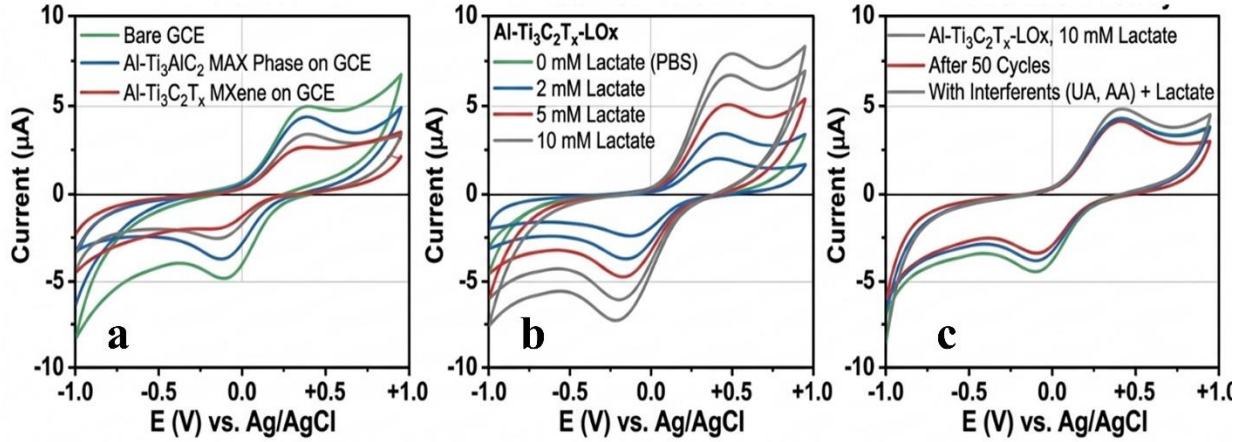

Figure 6 : Cyclic voltametric characterization of the Al–$Ti_3C_2T_x$ MXene-based lactate biosensor. (A) Comparison of electrochemical responses of bare GCE, Al–Ti_3AlC_2 MAX phase-modified GCE, and Al–$Ti_3C_2T_x$ MXene-modified GCE. (B) Concentration-dependent CV responses of the Al–$Ti_3C_2T_x$–LOx electrode toward lactate (0–10 mM). (C) Evaluation of operational stability after 50 cycles and selectivity in the presence of common interfering species (uric acid and ascorbic acid).

3.5 Effect of pH on the Electrochemical Response of the Al–$Ti_3C_2T_x$–LOx Lactate Biosensor

The electrochemical behaviour of the prepared Al–$Ti_3C_2T_x$–LOx biosensor was also studied using cyclic voltammetry in the pH range of 5.0–9.0. The activity of the enzyme as well as the electron-transfer kinetics depends greatly on the proton concentration of the electrolyte, thus optimal pH is required for obtaining the best sensing performance. The voltametric response of the biosensor was found to change considerably with respect to pH as illustrated in Figure 7(a).

Redox peaks were clearly detected throughout the pH range studied; the position of the peaks and the peak currents were significantly affected by the acidity of the electrolyte. The current responses were relatively low at pH = 5.0 with relatively low enzymatic activity and slower charge-transfer kinetics in acid conditions. The anodic peak current was significantly increased with increasing the pH from 5.0 to 7.0, indicating the improvement of the catalytic efficiency of LOx and favorable electron-transfer processes at the MXene-modified electrode surface. A decrease in current response was found at pH 7.5 and 8.0 while a slight recovery was found at pH 9.0 as pH increases beyond 7.0. The observed variations suggest that proton availability is an important factor in controlling both the enzymatic activities and the redox activities of the sensing system. The quantitative relationship between pH and peak current is shown in Figure 7(b).

The current increased slightly with an increase in pH from approximately 0.045 μA at pH 5.0 to a maximum current of approximately 0.112 μA at pH 6.5–7.0, which suggests that the electrochemical lactate detection is the best in near-neutral conditions. This enhanced response is due to the maintenance of the native structure of lactate oxidase and efficient electron transfer between the enzyme active sites and conductive Al–$Ti_3C_2T_x$ MXene matrix. A lower current was seen at higher pH, around 0.058 μA at pH 8.0, which could be due to changes in the structure of the enzymes, decrease in catalytic efficiency and a change in the surface charge characteristics of the electrode. A slight rise was noted at pH 9.0, but the current remained well below the optimum resulted at neutral conditions.

From these results, pH 7.0 was chosen as the optimum working pH for further electrochemical studies. The results showed that the fabricated Al–$Ti_3C_2T_x$–LOx biosensor was highly electrocatalytic under physiological conditions, which is significantly beneficial in practical applications for lactate determination in biological and clinical samples. The pH dependent behavior was also observed, further confirming the successful integration of the enzyme with the MXene platform as well as the role of proton-assisted charge-transfer mechanism in the sensing process.

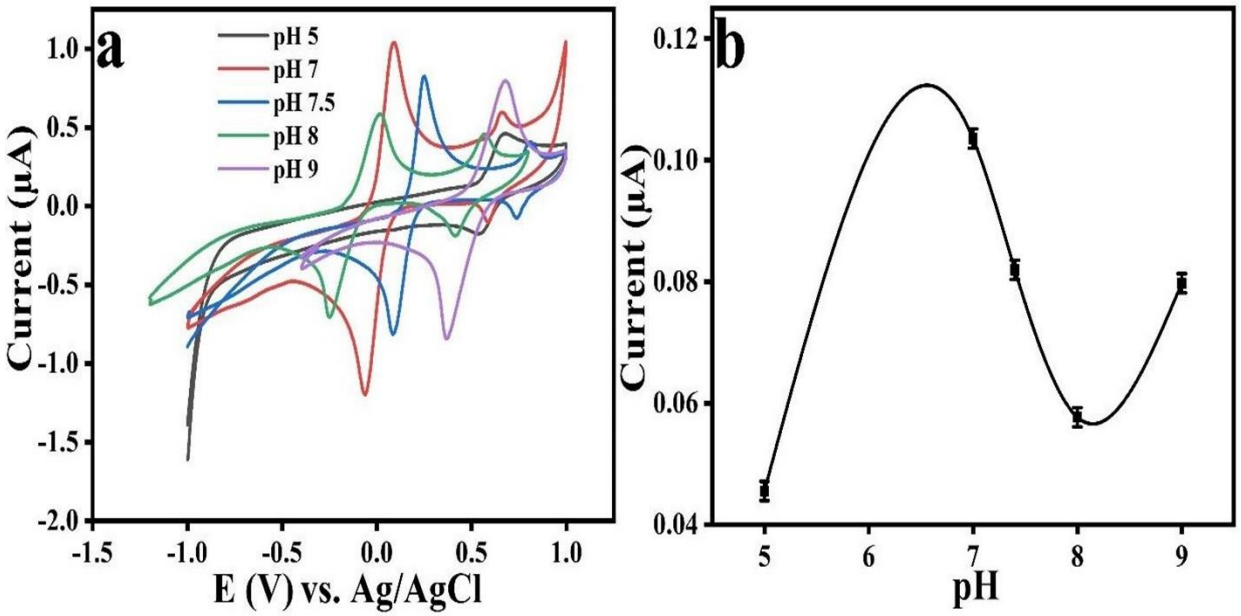

Figure 7: Effect of pH on the electrochemical performance of the Al–$Ti_3C_2T_x$–LOx lactate biosensor. (a) Cyclic voltammograms recorded at different pH values (5.0–9.0) demonstrating the influence of proton concentration on the redox behavior of the bioelectrode. (b) Variation of peak current as a function of pH, showing maximum current response near neutral conditions. Error bars represent standard deviation from replicate measurements.

3.6

3.7 Scan Rate Studies

Cyclic voltammograms were performed on the Al–$Ti_3C_2T_x$–LOx biosensor at scan rate between 20-200 mV $s^{-}1$ to study the electrochemical behavior of the biosensor. From the scan rate studies, it is concluded that the charge-transfer mechanism, the electron transfer rate and the electron transfer process is diffusion or surface confined reaction determine the scan rate. The anodic and cathodic peak currents increased consistently with the increase in the scan rate from 20 to 200 mV s^{-1} as illustrated in Figure 8(a). At the same time, the shift of peak potentials was also noticed which is a typical feature of quasi-reversible electrochemical systems.

The improvements in the current response as the scan rate was increased suggests that electron transfer rates are faster and the electrochemical communication between the immobilized lactate oxidase and the conductive Al–$Ti_3C_2T_x$ MXene matrix is effective. The sharp and symmetrical redox peaks further confirm the good electrochemical stability of the modified electrode and the immobilization of the biorecognition element on the surface of the MXene. Figure 8(b) shows the peak current of the results as functions of the scan rate. The anodic peak current (Ipa) and cathodic peak current (Ipc) all showed linear with increase in scan rate, which indicates that the electrochemical response is strongly dependent on rate of potential sweep. The high linearity is a sign of the efficient electron transport from one layer to another in the MXene structure, as well as the electroactive nature of the modified electrode. This is a typical characteristic of electrochemical systems with many available surface-active sites and fast charge-transfer pathways. Logarithmic plots of peak current against scan rate were also made to further explain the charge-transfer mechanism, which is shown in Figure 8(c). For both anodic and cathodic processes, a linear relationship was found, indicating that the electrochemical reaction has predictable kinetic behavior in the range of scan rates studied.

The slopes of the log–log plots were near unity, signifying that the redox process is essentially

surface-controlled, as opposed to diffusion controlled. This behavior is in line with the scenario of enzyme molecules being immobilized on the electrode surface, and undergoing electron transfer directly through the conductive network of MXenes. The two-dimensional layered structure of Al-$Ti_3C_2T_x$ MXene offers a large number of active sites and allows for very efficient charge transport, reducing the diffusion limitations. The scan rate dependence observed confirms the good electrochemical properties of the synthesized MXene platform and its potential for biosensing applications.

As revealed by their electron-transfer characteristics, electrochemical response and stability, the Al–$Ti_3C_2T_x$–LOx bioelectrode is effectively used for the sensitive and stable detection of lactate. The results further highlight the potential of MXene as an effective transducer material and its effectiveness for improving performance of biosensors by providing improved electrical conductivity and enhancing the electroactive surface area. The stability of Al–$Ti_3C_2T_x$–LOx Lactate Biosensor was evaluated.The stability of Al–$Ti_3C_2T_x$–LOx Lactate Biosensor was examined.

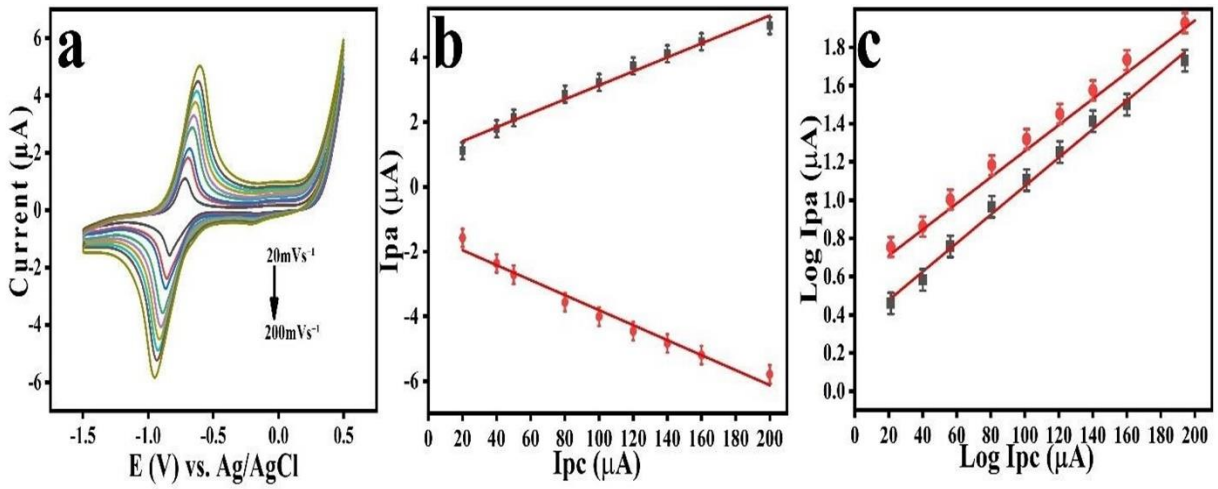

Figure 8: Scan rate-dependent electrochemical characterization of the Al–$Ti_3C_2T_x$–LOx lactate biosensor. (a) Cyclic voltammograms recorded at scan rates ranging from 20 to 200 mV s^{-1}, showing progressive increases in anodic and cathodic peak currents with increasing scan rate. (b) Linear relationship between peak currents and scan rate, indicating efficient charge-transfer kinetics. (c) Logarithmic plots of peak current versus scan rate used to evaluate the electrochemical mechanism.

3.8 Stability of the Al–$Ti_3C_2T_x$–LOx Lactate Biosensor

The electrochemical stability of the developed Al–$Ti_3C_2T_x$–LOx biosensor was assessed by successive cyclic voltammograms (CVs) with the same experimental conditions. One of the major parameters of performance is stability in biosensor applications which indicates the electrode's ability to show the same electrochemical activity over repeated use. The repeated CVs performed in the test showed a high degree of agreement with negligible differences in peak current and peak potential as seen in Figure 9. The electrochemical properties of the biosensor were well preserved over the testing period as, the anodic and cathodic redox peaks were clear and sharp.

The slight decrease in the current response indicates that the immobilized lactate oxidase still had catalytic activity and that it did not leach off the surface of Al–$Ti_3C_2T_x$ nor was it deactivated by the presence of the MXene. The unique structural and physicochemical properties of the MXene platform are responsible for the excellent stability. The two-dimensional structure of Al–$Ti_3C_2T_x$ allows the immobilization of enzymes onto its surface with a large surface area, and its

high electrical conductivity is beneficial for electron transfer between the enzyme active sites and the electrode surface. Moreover, MXenes are characterized by numerous surface functional groups which are able to mediate strong interactions with biomolecules leading to high enzyme retention and maintenance of bioactivity during repetitive electrochemical cycling.

The almost complete identical voltametric responses shown over several scans suggest structural integrity and electrochemical functionality of the electrode architecture when operated continuously. There is no significant peak broadening, peak shifting or current loss, indicating excellent resistance to surface fouling and degradation. The results validate the high performance of the Al–$Ti_3C_2T_x$–LOx bioelectrode and show that the bioelectrode is appropriate for long-term and repeated lactate sensing. The stability study overall shows that the synthesized MXene is an effective and stable biosensing platform. The repeatability of electrochemical response from repeated measurements, confirms the good operational stability of the biosensor, which is a promising tool for clinical, biomedical and physiological applications for lactate measurement. To analyze the detected lactate levels quantitatively.To quantitatively analyze the detected levels of lactate.

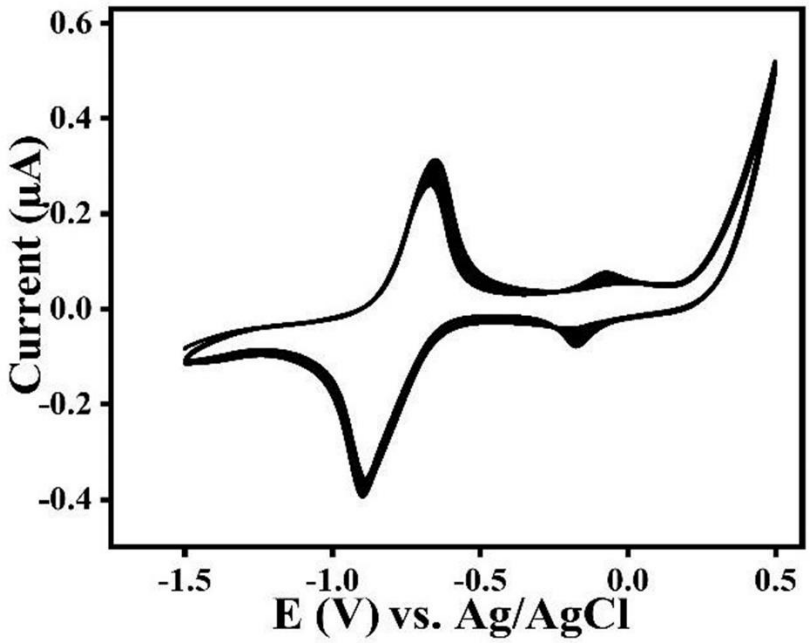

Figure 9 :Stability assessment of the Al–$Ti_3C_2T_x$–LOx lactate biosensor using repeated cyclic voltammetric measurements. The substantial overlap of successive voltammograms indicates excellent operational stability, preservation of enzymatic activity, and sustained electron-transfer performance of the MXene-based bioelectrode.

3.9

3.10 Quantitative Analysis of Lactate Detection

Analytical performance of the Al–$Ti_3C_2T_x$–LOx biosensor to lactate detection was evaluated by recording cyclic voltammograms for various lactate concentrations (10–90 µM). The voltametric responses and calibration curve corresponding to the above are shown in Figure 10(a–b). As can be seen in Figure 10(a), the oxidation current was systematically increased as the concentration of lactate was increased, thus the electrocatalytic activity of the biosensor is concentration dependent. Progressive improvement of anodic current due to the efficient enzymatic oxidation of lactate molecules and fast electron transfer

through the conductive Al–$Ti_3C_2T_x$ network of MXenes.

The electrochemical behavior of lactate and the generation of well-defined redox peaks indicated stable electrochemical behavior and good interaction of lactate molecules with the immobilized lactate oxidase over the range of concentrations studied. The bioelectrode shows the high affinity to lactate judging from the slow increase in peak current with concentration, and excellent analytical sensitivity.The calibration plot shown in Figure 10(b) reveals a strong linear relationship between lactate concentration and peak current response over the investigated range of 10–90 µM. Linear regression analysis yielded the following calibration equation:

$$I(\mu A) = 2.40 + 0.017C(\mu M)$$

with a correlation coefficient of

$$R2 = 0.987$$

indicating excellent linearity and reliable quantitative performance. The high correlation coefficient confirms that the generated electrochemical signal is directly proportional to lactate concentration within the studied range.

The analytical sensitivity of the biosensor was calculated from the slope of the calibration curve and was found to be approximately:

$$0.017 \mu A \mu M - 1$$

which reflects the ability of the Al–$Ti_3C_2T_x$ MXene platform to efficiently transduce small concentration changes into measurable electrical signals. The enhanced sensitivity can be attributed to the large electroactive surface area, excellent electrical conductivity, and abundant functional groups of the MXene nanosheets, which facilitate rapid electron transfer and effective enzyme immobilization.

The limit of detection (LOD) and limit of quantification (LOQ) were estimated according to the standard analytical expressions:

$$LOD = \frac{3\sigma}{S}$$

$$LOQ = \frac{10\sigma}{S}$$

where σ is the standard deviation of the blank signal and S is the slope of the calibration curve. Based on the experimental data, the biosensor exhibited an estimated LOD of 2.5 µM and LOQ of 8.3 µM, demonstrating its capability to detect low concentrations of lactate with high precision.

The favorable analytical characteristics obtained from the calibration study indicate that the fabricated Al–$Ti_3C_2T_x$–LOx biosensor possesses excellent quantitative performance. The combination of a wide linear range, low detection limit, high sensitivity, and strong linearity highlights the effectiveness of the MXene-based sensing platform for accurate lactate determination. These characteristics make the developed biosensor highly suitable for clinical diagnostics, sports physiology monitoring, and biomedical analysis where rapid and reliable lactate detection is required.

Table 1: Analytical Parameters of the Al–$Ti_3C_2T_x$–LOx Lactate Biosensor

Parameter	Value
Linear range	10–90 µM
Regression equation	I = 2.40 + 0.017C
Correlation coefficient (R^2)	0.987
Sensitivity	0.017 µA μM^{-1}
Limit of Detection (LOD)	2.5 µM
Limit of Quantification (LOQ)	8.3 µM

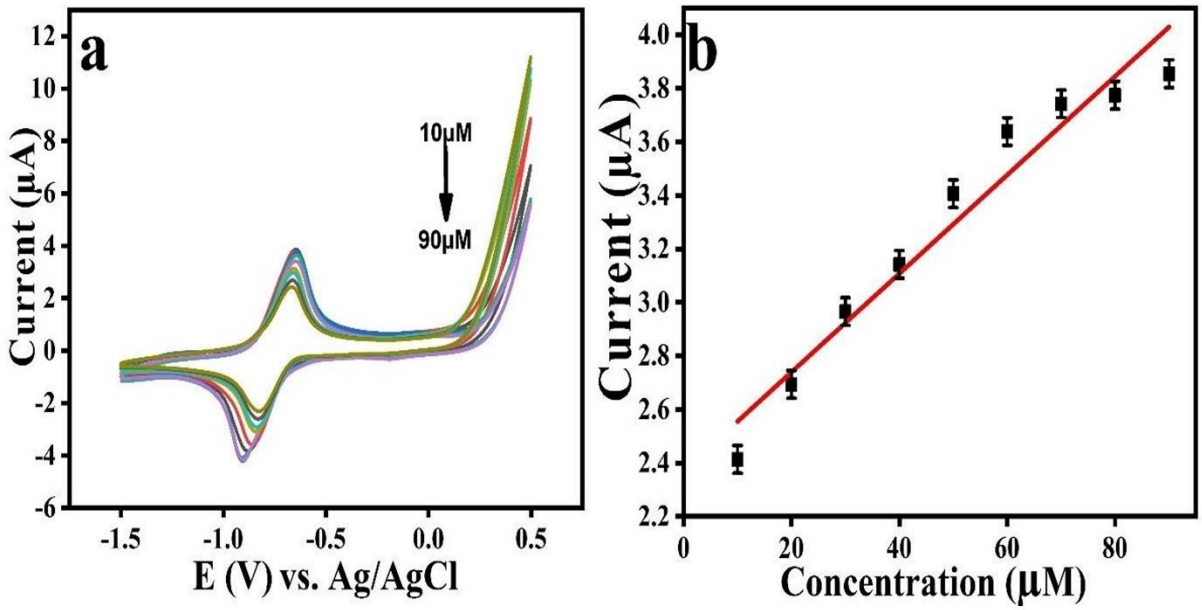

Figure 10 :Quantitative electrochemical determination of lactate using the Al–$Ti_3C_2T_x$–LOx biosensor. (a) Cyclic voltammograms recorded at lactate concentrations ranging from 10 to 90 μM, showing a progressive increase in oxidation current with increasing analyte concentration. (b) Calibration curve illustrating the linear relationship between peak current and lactate concentration. Error bars represent standard deviations of replicate measurements.

4 Conclusion

The Al-$Ti_3C_2T_x$ (MXene) was successfully synthesized from the Ti_3AlC_2 MAX phase by selective hydrofluoric acid etching, exfoliation and purification process in this study. The structural characterisation verified the successful conversion of the parent MAX phase to the two-dimensional MXene structure. The XRD spectra showed the typical shift of the diffraction peak (002) toward lower diffraction angle and the decrease of the higher order MAX phase reflections, which suggests an increase of interlayer spacing and showed successful removal of Al-layers. SEM showed that the MAX-phase morphology evolved to compact accordion-like multilayered structures with enlarged galleries between the layers, whereas EDS and elemental mapping analyses confirmed that Ti and C dominated the structure and that the O and F terminations were uniformly distributed on the surface while no aluminum was found.

The synthesized Al–$Ti_3C_2T_x$ MXene had a good physicochemical property which is very desired for electrochemical biosensing application. Cyclic voltammetry results showed increased electron transfer ability and greatly increased electrochemical activity when compared to the pristine MAX phase and blank electrode. The lactate biosensor based on MXenes showed a current response that was highly dependent on the concentration of lactate, good operational stability and high tolerance against common electroactive interferences. Optimization studies of pH and the scan rate yielded maximum performance at physiological pH (≈7.0) and a highly surface-controlled electron-transfer process in the highly conductive framework of MXene, supporting the results.

Quantitative electrochemical measurement revealed a good linear range of lactate detection between 10 and 90 μM, correlation coefficient (R^2) of 0.987, a sensitivity of 0.017 μA μM−1, a LOD of 2.5 μM, and a LOQ of 8.3 μM. These analytical parameters show the high sensitivity and accuracy of Al–$Ti_3C_2T_x$–LOx bioelectrode for detecting low lactate concentration levels. In summary, the

results indicate that Al–$Ti_3C_2T_x$ MXene has a combination of properties such as high electrical conductivity, enlarged interlayer spacing, high amount of surface functional groups, and excellent biocompatibility that make it suitable as an attractive platform for enzyme immobilization and electrochemical signal transduction applications. The fabricated MXene based biosensing system holds great promise for future wearable biomedical sensing applications, physiological assessment, clinical diagnostics, and regenerative lactate monitoring. Further work could involve the incorporation of the MXene platform into flexible sensing systems and its application in real biological samples for assessing its functionality in real-life biomedical applications.

REFERENCES

Ding, Y., et al., *A comprehensive review of advanced lactate biosensor materials, methods, and applications in modern healthcare.* Sensors, 2025. **25**(4): p. 1045.

Nasu, Y., et al., *Lactate biosensors for spectrally and spatially multiplexed fluorescence imaging.* Nature communications, 2023. **14**(1): p. 6598.

Xuan, X., et al., *Lactate biosensing for reliable on-body sweat analysis.* ACS sensors, 2021. **6**(7): p. 2763-2771.

Saleem, T., et al., *Medicinal plants mediated metal-based nanoparticles for biomedical applications and environmental remediation: A review.* Frontiers in Chemical Sciences, 2024. **5**(1): p. 18-35.

Rattu, G., et al., *Lactate detection sensors for food, clinical and biological applications: A review.* Environmental Chemistry Letters, 2021. **19**(2): p. 1135-1152.

Rasool, W., et al., *NATURAL POLYMER–BASED WASTEWATER TREATMENT USING PLANTAGO MAJOR SEED MUCILAGE: CHARACTERIZATION AND APPLICATION.* Spectrum of Engineering Sciences, 2026. **4**(1): p. 62-71.

Nasu, Y., et al., *A genetically encoded fluorescent biosensor for extracellular L-lactate.* Nature communications, 2021. **12**(1): p. 7058.

Malik, A., R.M.A. Bashir, and E. Ahmad, *A Systematic Review On the Occurrence, History, Effects, Analysis of POPs And its Future Aspects.* 2026.

Sainz, R., et al., *Lactate biosensing based on covalent immobilization of lactate oxidase onto chevron-like graphene nanoribbons via diazotization-coupling reaction.* Analytica Chimica Acta, 2022. **1208**: p. 339851.

Malik, W.M.A., et al., *Synergetic effect of heterostructure graphene oxide and Ce based metal organic framework nanocomposite as electrocatalyst for HER and OER.* Journal of Alloys and Compounds Communications, 2025. **7**: p. 100097.

Malik, W.M.A., et al., *RATIONAL DESIGN OF HIERARCHICAL MN/CO-NI/CO LAYERED DOUBLE HYDROXIDE HETEROSTRUCTURES AS BIFUNCTIONAL ELECTROCATALYSTS FOR HIGHLY EFFICIENT OVERALL WATER SPLITTING.* Spectrum of Engineering Sciences, 2026. **4**(5): p. 1858-1873.

Rasool, W. and W.M.A. Malik, *Optimized Adsorption of Sulfonamide Antibiotics from Milk Using Organically Modified Bentonite Clay.* Sustainable Environmental Insight, 2026. **3**(2): p. 170– 186-170– 186.

Chughtai, A.H., et al., *Designing a Heterogenous Bimetallic MOF (Pd/Cu-MOF) by Premade Linker Synthesis; an Efficient and Recyclable Catalyst for Cross-Coupling Reaction.* Topics in Catalysis, 2025: p. 1-16.

Noreen, F., et al., *Synthesis, in vitro, and in silico studies of 7-fluorochromone based thiosemicarbazones as α-glucosidase inhibitors.* Scientific Reports, 2025. **15**(1): p. 9816.

Ashraf, Z., et al., *One pot solvothermal synthesis of Zr-MOF and DNA-encapsulated Zr-MOF for improved current density towards OER.* Advances in nano research, 2025. **18**(6): p. 585-597.

Shoukat, W., et al., *Design, synthesis, characterization and biological screening of novel thiosemicarbazones and their derivatives with potent antibacterial and antidiabetic activities.* Journal of Molecular Structure, 2025. **1320**: p. 139614.

Ahmed Malik, W.M., et al., *A facile synthesis of CeO2 from the GO@ Ce-MOF precursor and its efficient performance in the oxygen evolution reaction.* Frontiers in chemistry, 2022. **10**: p. 996560.

Aldossary, H.B., S.M. Alsubaei, and G. AlZohbi. *MXenes: A New Frontier in Energy Storage Technology*. in *2025 5th International Conference on Electrical, Computer and Energy Technologies (ICECET)*. 2025. IEEE.

Kumar, S., et al., *Intercalant-free, restacking-suppressed single-layer $Ti_3C_2T_x$ MXene scaffolds for durable electrochemical energy storage.* Applied Materials Today, 2026. **50**: p. 103258.

Wu, B., et al., *Flux-grown large Ti3AlC2 single crystals with well-defined structural and electronic properties toward millimetre-scale MXenes.* npj 2D Materials and Applications, 2026.

JOHN, J., *Comparative Study of the Gas-Sensing Mechanisms in Functionalized Graphene and MXene Nanocomposite Films for CO_2 Detection*. 2025.

Gomha, S.M., et al., *Thiazole-based thiosemicarbazones: Synthesis, cytotoxicity evaluation and molecular docking study.* Drug design, development and therapy, 2021: p. 659-677.

Zahra, S.B., et al., *Synthesis of novel coumarin-based thiosemicarbazones and their implications in diabetic management via in-vitro and in-silico approaches.* Scientific reports, 2023. **13**(1): p. 18014.

Francis Verpoort, A., et al., *Wasif Mahmood Ahmed Malik, Abdul Ghafoor, Zohaib Ashraf, Muhammad Usman Akram, Muhammad Ibrahim. Enhanced electrochemical properties of single linker Cu-MOF for High-Performance water splitting application.* J. Emerg. Technol. Innov. Res, 2018. **11**: p. d846-d861.

Patil, P., et al., *Oxidative transformation of $Ti_3C_2T_x$ MXene on gamma radiation exposure in aqueous media.* npj 2D Materials and Applications, 2025. **9**(1): p. 99.

Cai, Z., et al., *Two-dimensional $Ti_3C_2T_x$ MXene integrated with nickel oxide for sensitive NH_3 sensing at room temperature.* Journal of Alloys and Compounds, 2025. **1036**: p. 181618.

Li, Y., et al., *Ethanol-induced stable dispersion and compatibility of MXene in WEP leading to highly ordered layered materials for high electromagnetic interference shielding performance.* Chemical Engineering Journal, 2026: p. 172688.

Yan, H., et al., *Construction of $Al/Ti_3C_2T_x$ composites via electrostatic self–assembly for visible–infrared camouflage applications.* Journal of Alloys and Compounds, 2025. **1010**: p. 177122.

Khan, M.H., P. Lamberti, and V. Tucci. *Hybrid Nanocomposite (Mxenes, Graphene, and Silicon) Anodes for Grid-Scale Lithium-Ion Batteries*. in *2025 IEEE International Conference on Environment and Electrical Engineering and 2025 IEEE Industrial and Commercial Power Systems Europe (EEEIC/I&CPS Europe)*. 2025. IEEE.

Soltani, O. and M.R. Jafari, *Strain-tunable electronic transport in MXenes for sensing and stable electronics.* Scientific Reports, 2026. **16**(1): p. 9355.

Chintakindi, J. and A. Mir, *Tailoring functionalization of Ti3C2 via tunable Electrochemical-Intercalation-Etching (EIE) route for enhanced electrochemical performance.* Chemical Engineering Journal, 2025: p. 169694.

Liang, C., et al., *Silk fibroin/poly (L-lactic acid) Janus nanofibre membranes enhanced with Al–$Ti_3C_2T_x$ MXene for dual-modal conductive and NIR-photothermal synergistic therapy of infected diabetic wounds.* International Journal of Biological Macromolecules, 2025: p. 149207.

Cai, Z. and H. Kim, *Recent advances in MXene gas sensors: synthesis, composites, and mechanisms.* npj 2D Materials and Applications, 2025. **9**(1): p. 66.